Journal of Ceramic Processing Research. Vol. 14, No. 4, pp. 513~516 (2013)

J O U R N A L O F
Ceramic Processing Research

Fabrication of the porous hydroxyapatite implant by 3D printing

Chao Qian and Jian Sun*

Department of Prosthodontics, Ninth People's Hospital, Shanghai Jiao Tong University School of Medicine, Shanghai Key Laboratory of Stomatology. Shanghai 200011, China

The feasibility of the preparation of porous hydroxyapatite (HA) implant by three-dimensional printing (3DP) was evaluated in the study. The nanoscale HA powders were blended with a water soluble binder to form the implant. The HA implants were divided into two groups according to the bonding area. The bonding area of group one was reserved to 100% in each layer, while the group two was reserved to 80%. The porous HA implant prototypes were fabricated by 3DP and sintered at 1250 °C. The porous HA implants were chemically stable and well crystallized after the sintering process with no distortion, showing an interconnected porous structure. The 80% HA implants had relatively larger pore size (100-200 μm) than 100% HA implant (50-150 μm). The sintered 100% and 80% HA implants had porosity of 58.58%-68.18% and compressive strength of 84.3-50.9 MPa. The properties of the porous HA implants matched well with bone tissue and exhibited excellent biomechanical compatibility.

Key words: Solid freeform fabrication, Porous materials, Composites, Microstructure.

Introduction

Hydroxyapatite (HA), as the similar chemical and structure to natural bone, is extensively accepted to be capable of osteoconduction and osteoinduction, leading to the widespread use of this material in clinical applications as bone substitute material [1-3].

Recently, porous implant materials have been regarded as the ideal implant materials which will permit and encourage new cells to attach, penetrate and grow with the firm and safe bind between implant and natural bone, therefore preventing the failure of the implant by loosening and movement [2, 5, 6].

Currently, the porous HA implants are usually fabricated by various conventional methods. However, these traditional processing methods have their limitation in the production of complex three dimensional specimens [4, 6]. Three-dimensional printing (3DP) process is one of the flexible solid freeform fabrication (SFF) technologies. It is defined as the additive fabrication method building three dimensional frameworks layer by layer with the aid of computer. The technology is suitable for highly complex three dimensional specimens free of mold [7]. With the advantage of versatility and simplicity, the 3D printing allows a wide array of solution and powder materials to process including metals, ceramics and polymers. The processing parameters can be controlled to produce complex shape and good tolerance of the final prototype [1, 2, 6, 7].

This method has already attracted a mass of scientific research to focus on customized biomaterial fabrication, especially on the porous implant [1, 6, 8]. In this study, special porous implant CAD models (STL file) with 100% and 80% nanoscale HA powder bonded on each slice were designed. According to the designed CAD models, porous HA implants were fabricated by 3DP. After sintering, microstructure, XRD and mechanical properties were evaluated and analyzed to investigate the feasibility and potential for 3DP fabrication of customized porous HA implant.

*Corresponding author:
Tel : +008621-23271699
E-mail: doctorsunjian74@yahoo.com.cn

Materials and Methods

Generation of the initial porous HA implant prototype

Printing of the porous HA implant prototype

The 3D printer is mainly composed of a Z-axis work station, a printing system, a Y-axis and a powder dispenser. The printing system and the powder dispenser move along the Y-axis from left to right to lay a layer of powders on the Z-axis work station. Then, after the Z-axis moves down one layer, the printing system goes back along the Y-axis. While it is moving, it prints the binder according to the graphic design of the implant's cross-section. The machine works in cycles and prints layer-by-layer till the 3D-structured prototype is completed. The maximum travel distance of the printing system are 200 mm in both X and Z directions, while it is 250 mm in Y direction.

HA powders (40 nm diameter, Aipu Nanomaterial Ltd, China.) and the binder, 10% polyvinyl alcohol (PVA, mesh size: 120) solution, were mixed at a ratio of 10 : 1 (mass) and carefully filled in the supply chamber of the 3D rapid prototype printer (LTY series, Shanghai Fochif Mechatronics Technology, Co, Ltd.).

Polyvinylpyrrolidone (PVP) as the penetration enhancer was dissolved in distilled water at the concentration of 0.05% and then poured into the supply chamber.

The porous HA implants were divided into two groups. Group one was the implant with the 100% combined area in each layer and group two was the 80% combined area. Each group involved five porous HA prototypes.

The scanning rate in X direction was set up as 0.4 m/s and the scanning space in Y direction was 0.2 m/s. The spinning rate of the powder dispenser was about 250 r/min. The implant cylinder grew along the long axis. Each printed layer was 0.1 mm in thickness after two cycles of printing. All the porous HA implant prototypes were printed and formed by 3D printing technology according to a graphic design in STL (surface tessellation language) format with 25 mm in diameter and 20 mm in height.

After building, a total of 10 porous HA implant prototypes were left in the machine for desiccation for 2 hrs and taken outside, left air-dried at room temperature for 24 hrs. They removed the unbound powders to complete fabrication.

Sintering of the porous HA implant prototype

After the fabrication, the porous HA implant prototypes were sintered at the optimum condition (1250, in the air condition) confirmed in the sintering study. The sintering program consisted of a slow heating rate to 500 ºC followed by a first plateau to burn the binder, and a faster heating rate to the temperature of 1250 ºC followed by a second plateau to sinter the prototype.

Performance test

Apparent porosity of sintered porous HA implant was measured by the Archimedes principle according to ASTM C373. A precision balance (XB124, Cany Precision Instruments Co. Ltd. Shanghai, China) was used to measure dry weight (W1). The specimen was soaked for 24 h after submerging and boiling in water for 3 hrs. The suspended weight in water (W2) was measured. After being taken out, the specimen removed the excess water in air by blotting with tissue paper and immediately reweighed (W3). The apparent porosity was calculated by the equation:

$$\text{Apparent porosity}(\%) = \frac{W3 - W1}{W3 - W2} \times 100 \quad (1)$$

The microstructure of the porous HA implant was evaluated with an environmental scanning electron microscope (JSM-6700F, Japan) at low vacuum and low voltage (10.0 kV). Prior to the observation, all the samples should be gold-sputtered. XRD analysis was applied to acquire the phase composition of the porous HA implant with a powder X-ray diffractometer (D8 advance, Bruker AXS, GMBH). The parameter was set up with 2s per step for counting time, 0.02º in moving step size and a range from 10 to 60º (2θ values) to collect the diffraction data.

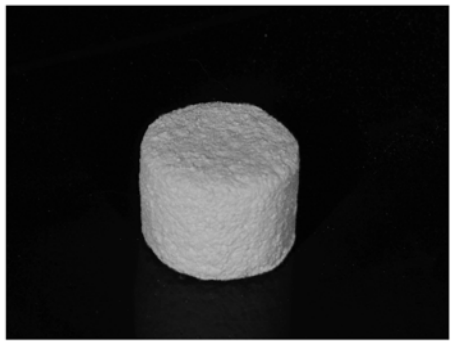

Fig. 1. 100% HA sintered under 1250.

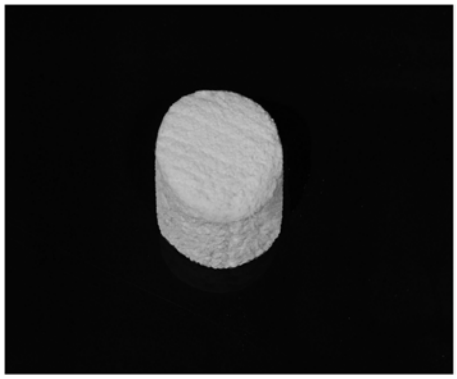

Fig. 2. 80% HA sintered under 1250.

The compression test of porous HA implant to analyze the mechanical properties was performed by a universal testing machine (Z100, Zwick GmbH, Ulm, Germany) at room temperature. The test was conducted with a constant strain rate of 2 mm/min.

Results and Discussion

3D printing of the porous HA implants

The 3D printing, a layer-by-layer assembly technique, with its scalability and flexibility, enables manufacturing diverse type of scale, shape, structure specimens. Compared with conventional methods, the 3D printing has changed the pattern of traditional design and manufacture makes up for the defects of complex structure and automation. This method is particularly adapted for fabricating tissue engineering scaffold and biomaterial implants [4].

The surface of the 100% and 80% HA implant prototypes was clear and smooth with no crack and no shape change produced by 3D printing technology. Fig. 1 and Fig. 2 exhibited the sintered 100% and 80% HA implant formed with no collapse. The network porosity was still clear to be seen of the 80%HA implant. The sintered 100% HA implants were more compact than 80% HA in texture.

The print precision of three dimensional printer used in this study was 0.04 mm and the thickness of each layer was 0.1 mm. Because of granule diameter of the

powder, micron materials were arranged in a sparse and larger spacing between each layer during the printing process. The size of micron powder could not match the printing precision that affected the shape and strength of the final composites. Therefore, the nanoscale HA powders were selected in the study with the average diameter of 40 nm. Compared with micron-level of the same material, there could be more compact HA powder in the same area of the layers, which might not only enhance densification of the green body due to greater surface area but also improve sinter ability, leading to better mechanical properties. Moreover, nanoscale HA powders contributed to fine preparation of the prototype with clear surface and internal texture, and control of aperture size [9-11].

Apparent porosity measurement and microstructure of the porous HA implant

The apparent porosity of 100% HA and 80% HA implant measured by Archimedes principle was plotted in Table. 1. The average apparent porosity of sintered 100% HA implant and 80% HA implant were 68.18%, 58.58% respectively. Investigated by SEM, 100% and 80% HA implant demonstrated a clear crystallization after sintering. Compared with Fig. 3(a) and Fig. 3(b), the crystallization of 100% HA implant was tighter than 80% HA implant because of the pore less. The SEM results demonstrated that the HA implant showed interconnected porous structure. The 100% HA implant was higher in density compared with 80%HA implant. The 80% HA implant had a relatively larger pore size (100-200 μm) than that of 100% HA (50-150 μm), which might be due to the less bind area of each layer for 80% HA. According to the literature, the ideal porosity and porous size in bone implants was 30-90% and 75-250 μm respectively for cell growth [12-14]. Interconnectivity of pores was also a significant structural property affecting the migration and proliferation of cells [15-17]. Further research would be needed to focus on the porosity and the pore size of the HA implant by adjusting the parameter of the 3DP process.

Table 1. Apparent porosity and compressive strength of porous HA implants.

Composite	Porosity (%)	Compressive strength (MPa)
100%HA	58.58 ± 4.35%	84.3 ± 12.1 MPa
80%HA	68.18 ± 0.71%	50.9 ± 5.1 MPa

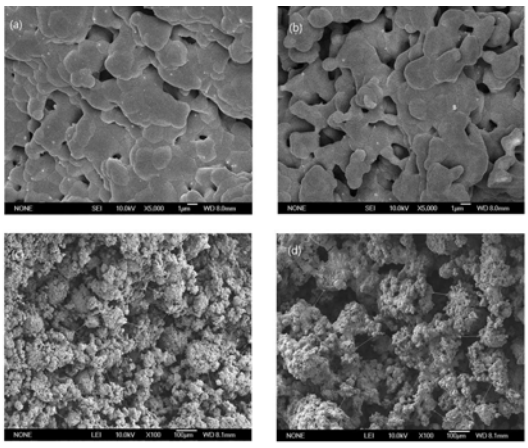

Fig. 3. SEM image of HA implants: (a) 100% HA implant, (b) 80% HA implant, (c) 100% HA implant, and (d) 80% HA implant.

XRD analysis

The XRD analysis of 100%HA and 80%HA implant processed by 3D printing performed after sintering (Fig. 4). The peak of the sintered 100%HA and 80%HA implants matched with the pure HA powder peak (JCPDS 9-432) and no shift of the HA characteristic peak was detected in the XRD analysis, indicating that the preparation and sintering process had no influent factors to the phase composition of HA implants.

Previous studies showed that HA sintered under 1000 ºC could not be well crystallized and bound with proper strength, while HA subjected to a further thermal starts to decompose into CaO, CaCO3 and TCP above 1300 ºC, and fully decomposed at approximately 1550 ºC [18-20]. In this study, the sintered HA implant subjected to 1250 ºC for 3 h after being sintered showed a XRD pattern with clear presence of HA and not related to the presence of CaO and CaCO3. The XRD result proved that the HA implants kept stable in element during the sintering process, and PVA completely decomposed after debinding process.

Compressive strength

Compressive strength achieved was 84.3 ± 12.1MPa for 100%HA implant, and 50.9 ± 5.1MPa for 80% HA implant (Table. 1). The less bind area of 80% HA implant, which reduced the compressive strength properties, but contrastingly increased the porosity and pore interconnectivity. According to literature, the compressive strength of trabecular bone was 2-12 MPa and that of cortical bone was 100-230 MPa respectively

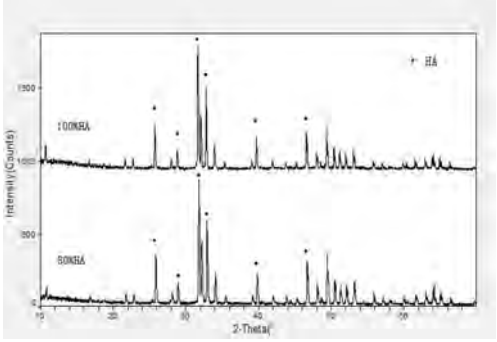

Fig. 4. XRD pattern of sintered 100% HA and 80% HA .

[21, 22]. The properties of porous HA implants were lower than native properties of cortical and higher than that of trabecular bone. Although the pores in the HA implant caused a relatively low compressive strength, it had been accepted by more and more researchers that they were beneficial for bone in-growth which made them suitable for bone substitute application [23-25].

Conclusion

In this study, 100% and 80% porous HA implants were successfully fabricated by 3DP and post-sintering. The following results were obtained:

1. It was observed that the porous HA implants had a clear crystallization after sintering and showed interconnected porous structure.

2. The porosity and pore size increased, while the compressive strength decreased with the decrease of the bind area of each layer of the porous HA implants.

3. The results demonstrated that fabrication of porous HA implants by 3DP was feasible, which had excellent biomechanical compatibility. Further research would be necessary to focus on the properties of the porous HA implant by adjusting the parameter of the 3DP process.

Acknowledgment

This study was supported by Natural Science Foundation of Shanghai (09ZR1416600) and Shanghai leading Academic Discipline Project (Project No. T0202, S30206).

References

1. M.P. Sanna, P.W. Ferry, W.G. Dirk, K. Minna, Ann. Med. 40 [4] (2008) 268-280.
2. W.Y. Yeong, C.K. Chua, K.F. Leong, C. Margam, Trends Biotechnol. 22 [12] (2004) 643-652.
3. B. Thomas, V. Mieke, S. Jorg, V.V. Sandra, D. Peter, Biomaterials. 33 [26] (2012) 6020-6041.
4. W.H. Zhong, F. Li, Z.G. Zhang. L.L. Song, Z.M. Li, Materials and Manufacturing Processes. 16 [1] (2001) 17-26.
5. T.B. Stephan, B. Hendrik, K. Oliver, S. Hermann, D. Timothy, S. Sureshan, W. Jorg, S. Eugene, H.W. Patrick, Oral Oncology. 45 [11] (2009) e181-e188.
6. U. Ben, S. Duane, A. Rhonda, G. Mark, Journal of Manufacturing Processes. 10 [2] (2008) 96-104.
7. S.G. Simranpreet, K. Munish. Materials and Manufacturing Processes. 24 [12] (2009) 1405-1411.
8. A. Butscher, M. Bohner, S. Hofmann, R. Gauckler, R. Muller, Acta Biomaterialia. 7 [3] (2011) 907-920.
9. J.A. Lewis, J.E. Smay, J. Stuecker, J. Cesarano, J. Am. Ceram. Soc. 89 [12] (2006) 3599-3609.
10. K.A. Gross, S.S. Saber., J. Aust. Ceram. Soc. 43 (2007) 98-101.
11. H.J. Zhou, L. Jaebeom, Acta Biomaterialia. 7 [7] (2011) 2769-2781.
12. S. Hajar, G. Debby, J.A. Wouter, F.V. Cornelus, V. Tina, E.H. Wim, Acta Biomaterialia. 7 [5] (2011) 1999-2006.
13. B.D. Boyan, T.W. Hummert, D.D. Dean, Z. Schwartz, Biomaterials. 17 [2] (1996) 137-146.
14. M.C. Doernberg, B.V. Rechenberg, M. Bohner, S. Grunenfelder, G.H. Lenthe, R. Muller, B. Gasser, R. Mathys, G. Baroud, J. Auer, Biomaterials. 27 [30] (2006) 5186-5198.
15. K.A. Hing, B. Annaz, S. Saeed, P.A. Revell, T. Buckland, J. Mater. Sci.: Mater. Med. 16 [5] (2005) 467-475.
16. B. Andre, B. Marc, R. Christian, E. Annika, H. Roman, D. Nicola, R.V. Philipp, M. Ralph, Acta Biomaterialia. 8 [1] (2012) 373-385.
17. K.A. Hing, S.M. Best, K.E. Tanner, W. Bonfield, P.A. Revell, J. Biomed. Mater. Res. A 68[1] (2002) 187?200.
18. C.J. Liao, F.H. Lin, K.S. Chen, J.S. Sun, Biomaterials. 20 [19] (1999) 1807-1813.
19. J.M. Zhou, X.D. Zhang, J.Y. Chen, S.X. Zeng, K. Groot, J. Mater. Sci.: Mater. Med. 4 [1] (1993) 83-85.
20. E. Saiz, L. Gremillard, G. Menendez, P. Miranda, K. Gryn, A.P. Tomsia, Materials Science and Engineering C. 27 [3] (2007) 546-550.
21. J.Y. Rho, T.Y. Tsui, G.M. Pharr, Biomaterials. 18 [20] (1997) 1325-1330.
22. C.H. Turner, J. Rho, Y. Takano, T.Y. Tsui, G.M. Pharr, J. Biomech. 32 [4] (1999) 437-441.
23. L. Stefan, C. Senan, B. Valerie, M. Peter, D. Lutz, K. Ludwika, B. Christine, I. Anita, Acta Biomaterialia. 8 [9] (2012) 3446-3456.
24. S.S. Saber, K.A. Gross, Acta Biomater. 5 [6] (2009) 2206-2212.
25. R.W. Joseph, J.H. Amanda, K.L. Sheeny, C.J. Park, W.M. Abby, A.C. Jo, G.C. Sherrie, B.W. Matthew, D.J. Russell, J.W. Amy, Biomaterial. 28 [1] (2007) 45-54.